Physica D 56 (1992) 1–22
North-Holland

PHYSICA D

Exact numerical studies of Hamiltonian maps: Iterating without roundoff error

David J.D. Earn
Institute of Astronomy, Madingley Road, Cambridge CB3 0HA, UK

and

Scott Tremaine
Canadian Institute for Theoretical Astrophysics, University of Toronto, Toronto, Canada M5S 1A1[1]
and Theoretical Astrophysics 130-33, California Institute of Technology, Pasadena, CA 91125, USA

Received 22 April 91
Revised manuscript received 21 November 91
Accepted 27 November 91
Communicated by R.S. MacKay

For many important Hamiltonian maps (e.g., the standard map) it is possible to construct related mappings that (i) carry a lattice into itself; (ii) approach the original map as the lattice spacing is decreased; (iii) can be iterated exactly using integer arithmetic; and (iv) are Hamiltonian themselves. We compare these lattice maps to maps that use floating-point arithmetic to evaluate the original map. We discuss the problems associated with roundoff error and we argue that lattice maps are superior to floating-point maps for the study of the long-term behaviour of Hamiltonian dynamical systems.

1. Introduction

The study of dynamics has been revolutionized by numerical studies of Hamiltonian maps using fast computers. However, most computers retain only a fixed number of digits and round real numbers to nearby representable numbers at every iteration of the map. The errors induced in this way can be a serious concern when examining the long-term behaviour of these maps; the cumulative effect of roundoff can lead to dramatic alterations in the long-term behaviour of the computed trajectories.

Roundoff error can be avoided by using integer arithmetic. A given Hamiltonian mapping H (i.e., a symplectic diffeomorphism) can be replaced by another Hamiltonian map H^* that maps a lattice to itself and approaches H as the lattice spacing is decreased. If the new map H^* has been suitably defined, and if the initial point is chosen on the lattice, integer arithmetic can be used to iterate it indefinitely without errors of any sort.

The use of lattice maps to approximate continuous Hamiltonian maps was pioneered by Rannou [24]. Rannou showed that phase portraits generated by repeated application of these lattice maps are very similar to those produced using corresponding floating-point maps, and that the similarity is not sensitive to the lattice spacing. She also argued that apparently chaotic motion observed with lattice maps is equivalent to the behaviour of a random mapping on a lattice.

[1] Permanent address.

Our emphasis is on long-term behaviour. The phase portraits after many iterations of floating-point maps can be very different from those generated with lattice maps, so the long-term behaviour predicted by each method of computation is not necessarily the same. This concern has motivated at least two authors to use lattice maps rather than floating-point maps for their research [16, 26]. It has also stimulated research into the effects of phase space discretization (e.g., ref. [23]).

In this paper we study two simple Hamiltonian maps. The first is two-dimensional and the second is four-dimensional. Focusing on the long-term behaviour of orbits, we compare our exact results obtained using integer arithmetic with those obtained using floating-point arithmetic. We also discuss more general $2N$-dimensional lattice maps and show that they can be used to construct an integration scheme for Hamiltonian flows that is exactly symplectic.

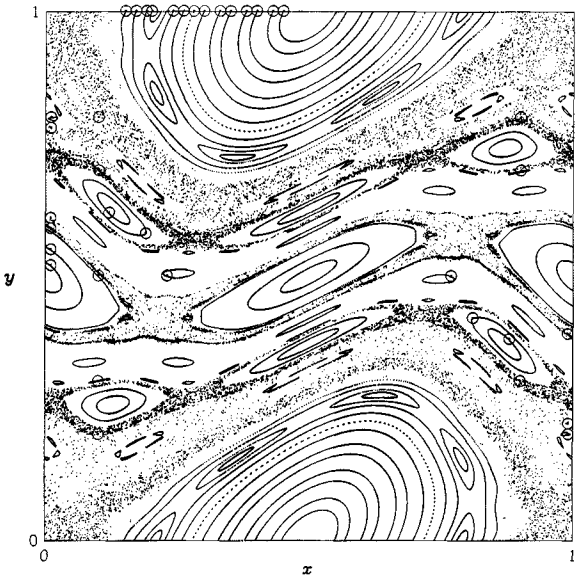

Fig. 1. A plot of the first 2000 points of 37 trajectories of the floating-point version R_4 of the standard map with $K = 1$. Initial points are marked with a circle, and are listed in table 1.

2. The standard map

One of the best known Hamiltonian maps is the standard map (e.g., ref. [20]). It can be written

$$x_{n+1} = x_n + y_{n+1},$$
$$y_{n+1} = y_n + \frac{K}{2\pi}\sin(2\pi x_n), \qquad (1)$$

where K is the stochasticity parameter. This map is periodic in both x and y. Modulo 1, it is a mapping on the unit square.

It is not possible to iterate the standard map exactly using finite-precision arithmetic. However, for a small number of iterations the effect of roundoff error is probably unimportant. Fig. 1 shows a plot of the first 2000 points of several trajectories computed by applying `REAL*4` (i.e., 4-byte floating-point arithmetic with precision $\sim 2^{-23} \approx 10^{-7}$) to (1) with $K = 1$. At each iteration, the computer finds the equivalent of y_{n+1} in the unit interval, uses this to find $x_{n+1} \pmod 1$ and plots the resulting point on the unit square.

Initially nearby chaotic trajectories separate exponentially fast, so without careful analysis it is not clear that the apparently chaotic trajectories in fig. 1 have anything to do with the standard map. Even regular trajectories are seriously affected by roundoff in the long term. We are interested in very large numbers of iterations so it is essential to determine what the bad effects of roundoff error are and how they can be avoided.

In order to be precise, we define R_b to be the standard map (1) as computed in `REAL*b` floating-point arithmetic on a given computer (in our case, a μVAX 3800). The map R_b carries the set of representable points (ordered pairs of representable numbers) into itself; the representable numbers are real numbers of the form

$$\pm \sum_{i=1}^{P} f_i 2^{e-i}, \qquad (2)$$

where P is a fixed integer, e is an integer in a fixed range, $f_1 = 1$, and $f_i \in \{0, 1\}$ for all i. For

VAX computers, $P = 24$ and $e \in \{-127, \ldots, 127\}$ in REAL*4 arithmetic. We let $\mathbb{P}_b$ denote the set of b-byte numbers representable in the given computer. If p_b and k_b denote the values of 2π and $K/2\pi$ as computed in REAL*b, then

$$R_b\begin{pmatrix} x \\ y \end{pmatrix} = \begin{pmatrix} x \oplus \{y \oplus [k_b \otimes \sin_b(p_b \otimes x)] \bmod_b 1\} \bmod_b 1 \\ y \oplus [k_b \otimes \sin_b(p_b \otimes x)] \bmod_b 1 \end{pmatrix}, \quad x, y \text{ representable}, \tag{3}$$

where $\otimes$ and $\oplus$ denote b-byte floating-point multiplication and addition, respectively. (Fig. 1 is strictly a plot of trajectories of R_4 rather than the standard map.) When iterating R_b, roundoff occurs at each multiplication and addition (including reduction modulo 1, which is why we write $\bmod_b$). Additional errors occur in the the approximate evaluation of the sine function but these can be treated simply as roundoff errors also, as we indicate with our notation $\sin_b$[#1].

Now consider a discrete subset of the plane, the lattice L_m with m points per unit vertically and horizontally. We shall construct a map from L_m to itself that can be iterated exactly using integer arithmetic. Letting $X = mx$ and $Y = my$, the standard map can be written

$$X_{n+1} = X_n + Y_{n+1},$$
$$Y_{n+1} = Y_n + \frac{m}{2\pi} K \sin\left(\frac{2\pi}{m} X_n\right). \tag{4}$$

(We are using the notation L_m to denote both the lattice with spacing $1/m$ and the lattice with unit spacing between points. Thus we view the transformation between (x, y) and (X, Y) as passive, leaving the plane fixed but changing the coordinates.) The lattice L_m is not an invariant subset of the map (4). However, if we replace $\frac{m}{2\pi} K \sin(\frac{2\pi}{m X})$ with a function $S_m(X)$ that takes integer values on lattice points, L_m will be an invariant subset of the new map. We define S_m on the lattice by

$$S_m(X) = \left[\frac{m}{2\pi} K \sin\left(\frac{2\pi}{m} X\right)\right], \quad X \text{ an integer}, \tag{5}$$

where square brackets denote the nearest integer to the representable number obtained by evaluating the expression with REAL*b arithmetic. (Normally we use $b = 8$ in evaluating eq. (5). Since we always use 4-byte integers, this virtually eliminates the influence of floating-point calculations on the definition of the lattice map.)

From (5) we define the new mapping

$$\begin{pmatrix} X_{n+1} \\ Y_{n+1} \end{pmatrix} \equiv I_m \begin{pmatrix} X_n \\ Y_n \end{pmatrix} = \begin{pmatrix} X_n + Y_n + S_m(X_n) \\ Y_n + S_m(X_n) \end{pmatrix}, \quad X_n, Y_n \text{ integers}. \tag{6}$$

Several trajectories of I_{1000} and I_{50} with stochasticity parameter $K = 1$ are shown (mod m) in figs.

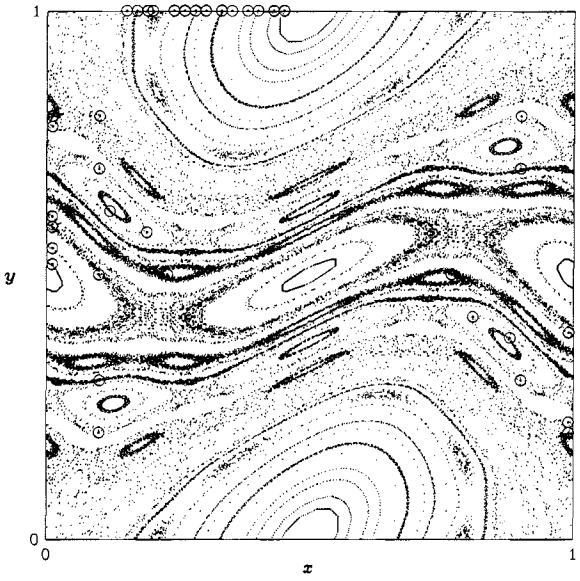

Fig. 2. Orbits starting at the same 37 initial points as in fig. 1, calculated using I_{1000} with $K = 1$. Every orbit shown is complete, i.e., every point is plotted until the trajectory returns to the initial point.

[#1] Errors in floating-point additions destroy the Hamiltonian properties in this map. Other errors are less important. See section 5.

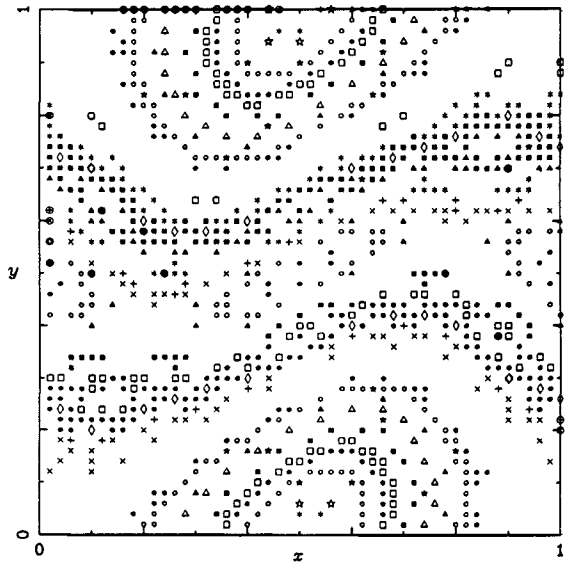

Fig. 3. Orbits of I_{50} with $K = 1$ and the same initial points as in figs. 1 and 2. Every orbit shown is complete; different orbits are plotted with different symbols. Note that due to the low resolution of the lattice L_{50} the 37 initial conditions used in figs. 1 and 2 give rise to only 31 distinct orbits of I_{50}; this occurs both because some initial conditions are not on the lattice L_{50}, and because some initial conditions lie on the same orbit of I_{50}.

2 and 3 respectively (note that the reduction modulo m can always be done exactly). It is interesting that the general structure of phase space is preserved for $m = 50$ and even coarser grids. Rannou [24], Smith [26] and Gonczi [13] have also investigated lattice versions of the standard map.

The map I_m approaches the standard map as m is increased (if the accuracy of the floating-point arithmetic used to evaluate the sine is also increased at an appropriate rate). Of course, the floating-point map R_b also approaches the standard map as b is increased. However, I_m can be extended to an area-preserving diffeomorphism (see section 5) so it is the restriction of this (continuous) Hamiltonian map[#2] to the lattice L_m. Since they can be extended to area-preserving maps on the whole phase space of interest (symplecticity is equivalent to preservation of area in two dimensions) we refer to the lattice maps I_m as Hamiltonian maps themselves. R_b, on the other hand, is not even one-to-one (see appendix) so it cannot be extended in this way and it does not necessarily share any of the important features of a Hamiltonian map.

It should be stressed that the difference between the standard map and the lattice map I_m is a small but rapidly varying perturbation. As the lattice spacing is decreased, the amplitude of the perturbation approaches zero but it varies more and more rapidly as a function of the phase space coordinates. Thus the KAM theorem (e.g., ref. [22]) does not guarantee that most invariant tori of the standard map survive this perturbation. Nevertheless, since it is Hamiltonian, this perturbation is likely to have less serious effects on the long-term behaviour of the map than the perturbation induced by using floating-point arithmetic to evaluate the original map.

[#2] In the notation of the introduction, H is the standard map (1) and H^* is the extension of I_m to an area-preserving diffeomorphism.

3. Long-term trajectories

Before discussing the results of our computations we consider what might be expected to go wrong when long-term calculations are performed using floating-point arithmetic.

We first define a few terms precisely. The trajectory from the point P under the map F is the set of points visited when F is iterated from P, i.e.,

$$\mathrm{traj}_F(P) = \{F^l(P): l = 0, 1, 2, \ldots\}.$$

The "preview" of the set S under the map F is the set of all points that eventually lead to a point in S upon iteration of F, i.e.,

$$\mathrm{prev}_F(S) = \bigcup_{l=1,2,\ldots} F^{-l}(S),$$

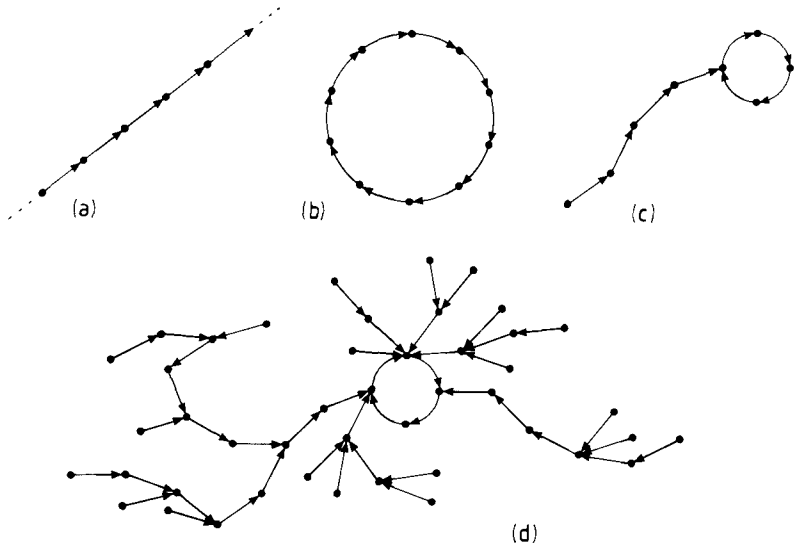

Fig. 4. Map-graphs as described in section 2.2. These graphs illustrate the possible complexity of map-graphs but do not correspond to any particular mapping. (a) A bi-infinite path. (b) A finite circuit, corresponding to a cycle in a Hamiltonian map or the limit circuit of a map using floating-point arithmetic. (c) The subgraph of a typical trajectory of a floating-point map. (d) A complete component of the map-graph of a floating-point map.

where $F^{-1}(S)$ is the set of all points that F maps into S. If $S = \{P\}$, a single point, we write $\mathrm{prev}_F(P)$ for $\mathrm{prev}_F(\{P\})$. The orbit of the map F that includes the point P is the set

$$\mathrm{orb}_F(P) = \mathrm{traj}_F(P) \cup \mathrm{prev}_F(\mathrm{traj}_F(P)).$$

If A is a set then F is A-invariant if $F(A) \subseteq A$.

Any iterated mapping F can be represented by a directed graph, which we call a "map-graph"[#3]. The vertices of the map-graph represent the points visited by the orbit and the edges represent the space between a point and its successor under F. There is a one-to-one correspondence between the orbits of F, as defined above, and the connected components of its map-graph. If F is one-to-one then each component has one of two forms; orbits are either bi-infinite paths or (finite) circuits (figs. 4a and 4b). Our lattice maps are one-to-one so all their orbits are of these two forms ($\mathrm{orb}_{I_m}(P) = \mathrm{traj}_{I_m^{-1}}(P) \cup \mathrm{traj}_{I_m}(P)$). However, since we plot the orbits modulo m, the sub-lattice on which we plot is finite and all the orbits appear to be circuits as in fig. 4b.

The situation is more complicated for many-to-one maps like R_b. The subgraph corresponding to a typical trajectory is drawn in fig. 4c. In general, such a subgraph will be a subset of a graph such as that shown in fig. 4d. All components of the map-graph of a many-to-one map on a finite set (such as $\mathbb{P}_b^2$) must contain exactly one circuit, but a tree may be connected to any number of vertices of this "limit circuit" (for any $P \in \mathbb{P}_b^2$, $\mathrm{prev}_{R_b}(P)$ may contain many branches). The portion of a trajectory that occurs before its limit circuit is reached is its "transient"[#4].

If R_b was the restriction to $\mathbb{P}_b^2$ of a $\mathbb{P}_b^2$-invariant Hamiltonian map, then each orbit of R_b would be a circuit on its map-graph, as in the case of $I_m \pmod m$. The effect of roundoff error

[#3] Such graphs have been studied previously. See refs. [6, 19], and for earlier work refs. [7, 15].

[#4] Implications of the fact that trajectories of floating-point maps lead to limit circuits are discussed in the context of one and two-dimensional dissipative maps in ref. [3] and more generally in ref. [2].

is to break many of these circuits and then connect up all the broken circuits to form map-graph components that resemble fig. 4d.

We can therefore anticipate that if we iterate a trajectory of R_4 starting from a point in a regular region of the phase plane of the standard map, the orbit will appear to drift from one invariant curve of the standard map to another, until it settles finally on a cycle (the limit circuit) on which it remains. Drifting across invariant curves never occurs in two-dimensional Hamiltonian maps; regular orbits are confined to individual KAM curves and chaotic orbits are bounded between KAM curves where they exist. Apparent drifting across curves can be misleading in general, of course, since invariant curves can have pathological structure; but the existence of limit circuits is a purely non-Hamiltonian feature of floating-point maps. How much "forbidden motion" is observable in one of our plots depends crucially on where on the map-graph like fig. 4d the orbit is initiated, and by how much we magnify the plot. We determine exactly when the limit circuit is reached, and precisely how long it is, using a simple algorithm of R.W. Floyd [1, 9, 17].

Figs. 5 and 6 show an example of the behaviour of a trajectory of R_4 (with $K = 1$) that begins in an apparently regular region. The initial point of the trajectory shown is $(x, y) = (0.26, 1)$. Fig. 5 shows the complete trajectory (i.e., every point is plotted until the limit circuit is completed); it appears to lie on an invariant curve. However, fig. 6 reveals more complex behaviour (a small region of the plot in fig. 5 is shown on a much larger scale). The trajectory appears to remain near a single invariant curve of the standard map for approximately 10^5 iterations (fig. 6a). More iterations show that the trajectory appears to drift across many distinct invariant curves (fig. 6b, 10^6 iterations; fig. 6c, 2.15×10^6 iterations) until settling after 2 148 397 iterations on a limit circuit of length only 1622 iterations. Only two points of the limit circuit appear in fig. 6d, which shows the same region as the other plots in fig. 6.

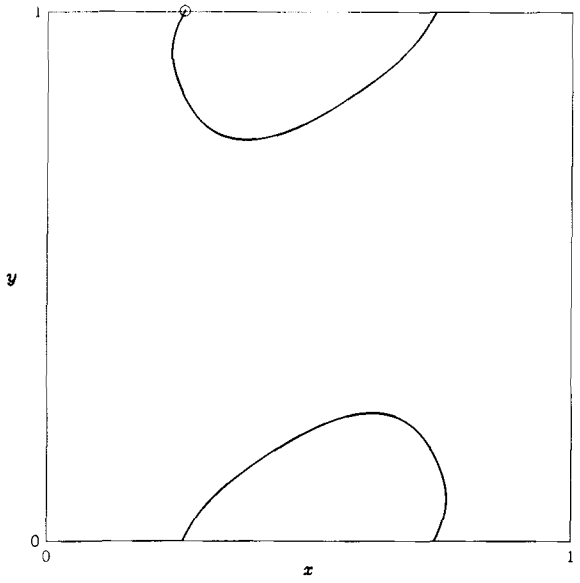

Fig. 5. A typical "regular" trajectory of the floating-point map R_4 with $K = 1$. The initial point of this orbit is $(x, y) = (0.26, 1.0)$. The complete trajectory is shown; it appears to remain on an invariant curve but fig. 6 reveals that the motion is more complicated.

Fig. 7 shows the trajectory beginning at the same point ($(x, y) = (0.26, 1)$) but iterated using the lattice maps I_{10^5}, I_{10^6}, I_{10^7}, and I_{10^8}. The scale is the same as in fig. 6. Throughout its evolution $\mathrm{traj}_{I_m}((0.26m, m))$, for any m, appears to remain near to a single invariant curve of the standard map. (The trajectories plotted in fig. 7 cover all of $\mathrm{orb}_{I_m}((0.26m, m))$ since we plot every point until the initial point is revisited.)

Since I_m is exactly Hamiltonian, the trajectories shown in fig. 7 do not cross invariant curves of I_m (although they may cross invariant curves of the standard map). They may or may not lie on invariant curves of I_m; if they do, then it is clear that the invariant curves must have quite pathological structure. From a practical point of view, the important features are that (i) the scatter in the integer map I_m (fig. 7) is much smaller than the scatter in the floating-point map R_4 (fig. 6), even for m as small as 10^5; (ii) the scatter in I_m decreases as m increases. Both these features

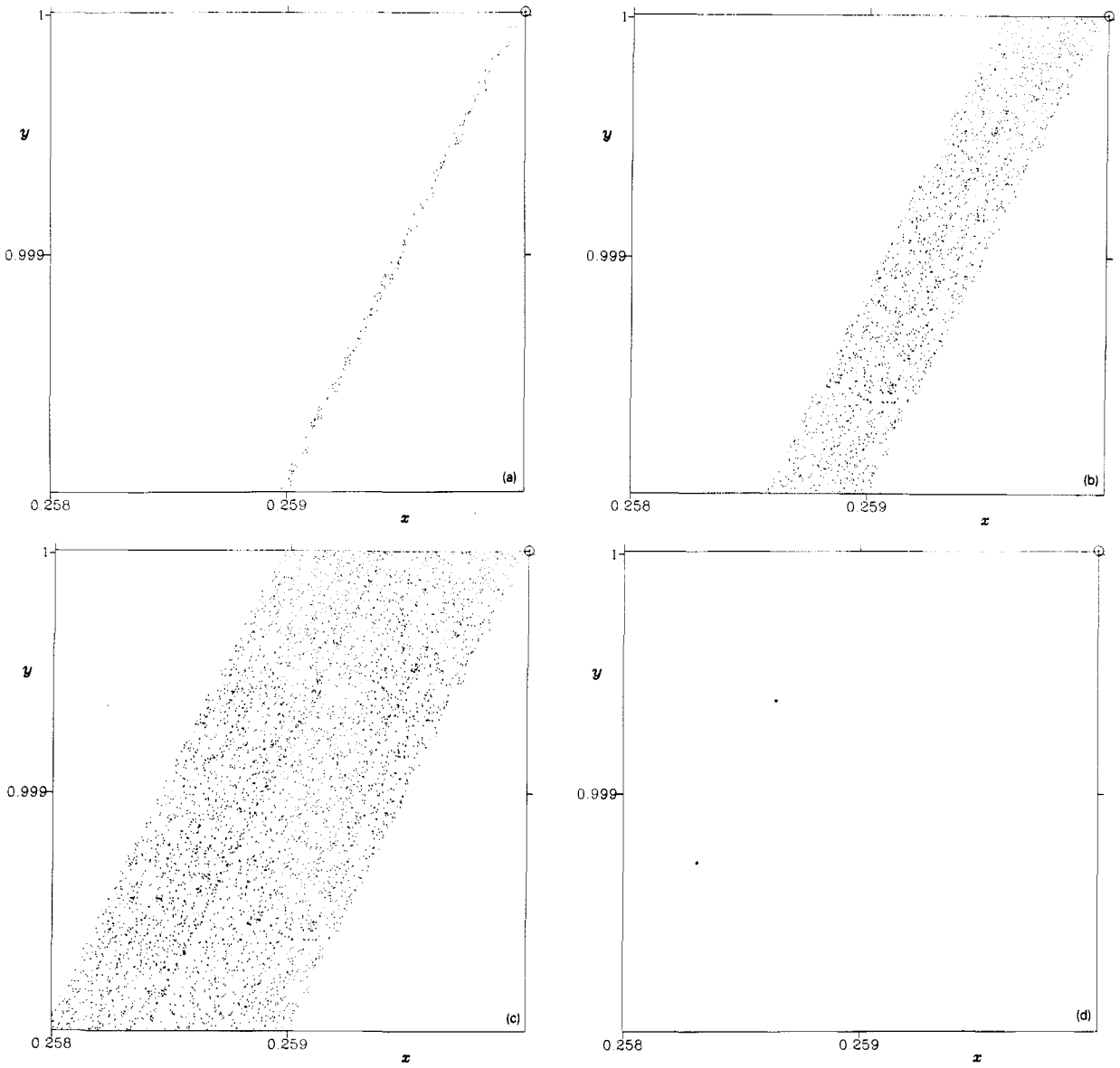

Fig. 6. Enlargements of a portion of fig. 5 at various stages of evolution of the trajectory. (a) 10^5 iterations. (b) 10^6 iterations. (c) 2150019 iterations. The limit circuit has been reached by this time and the plot is terminated after one completion of the limit circuit. (d) The limit circuit alone (1622 iterations). Only two points of the limit circuit appear in this enlargement, which is of the same region as (a), (b), and (c).

suggest strongly that I_m mimics the behaviour of the standard map better than floating-point maps.

We now comment on the meaning of regular and chaotic trajectories of a map defined on a finite set, whether the lattice (for lattice maps) or the representable points (for a floating-point map). In an obvious sense all orbits are "regular" since they are periodic (in the case of lattice maps) or at least lead to a periodic orbit (in the case of floating-point maps). However, Rannou [24] has argued convincingly that periodic orbits of a lattice map can be random in a very natural

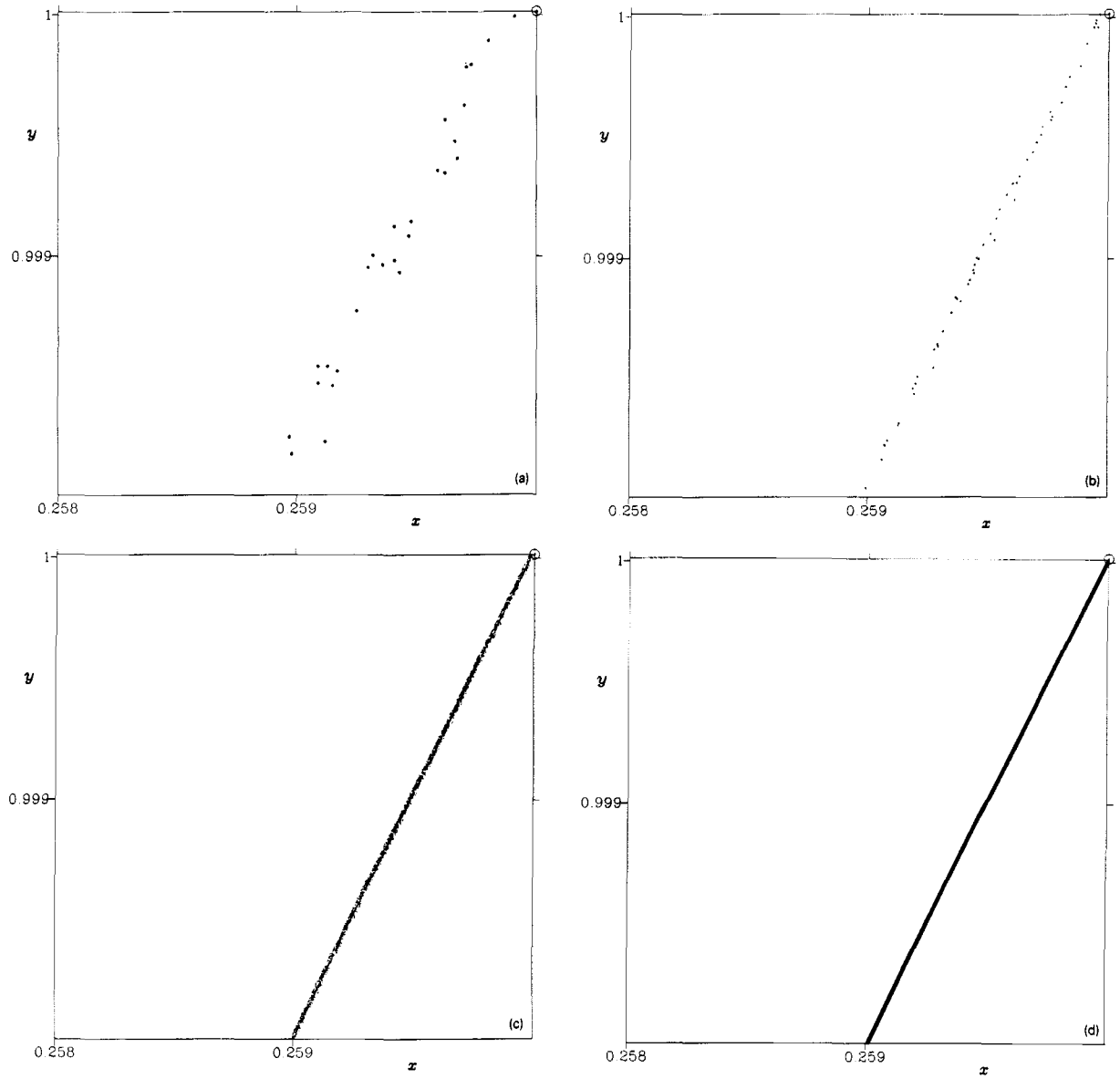

Fig. 7. Complete orbits of the mapping I_m started from the same point as the plots in figs. 5 and 6. The scale in these plots is the same as in fig. 6. (a) $m = 10^5$, cycle length $L = 16728$. (b) $m = 10^6$, $L = 34756$. (c) $m = 10^7$, $L = 1689794$. (d) $m = 10^8$, $L = 130141384$.

sense (i.e., the map is statistically indistinguishable from a random permutation of the lattice) so it is reasonable to label these orbits "chaotic" or "stochastic".

The most common method of quantifying chaos is to estimate the Lyapunov characteristic exponents (LCEs), i.e., mean exponential rates of divergence of nearby trajectories [4, 5]. Technically, the LCEs are the limits of the average rates of divergence as $t \to \infty$; we must hope that the limits can be established with adequate accuracy after a reasonable time. One might expect that approximations from longer studies would always provide more reliable LCE estimates, but floating-point

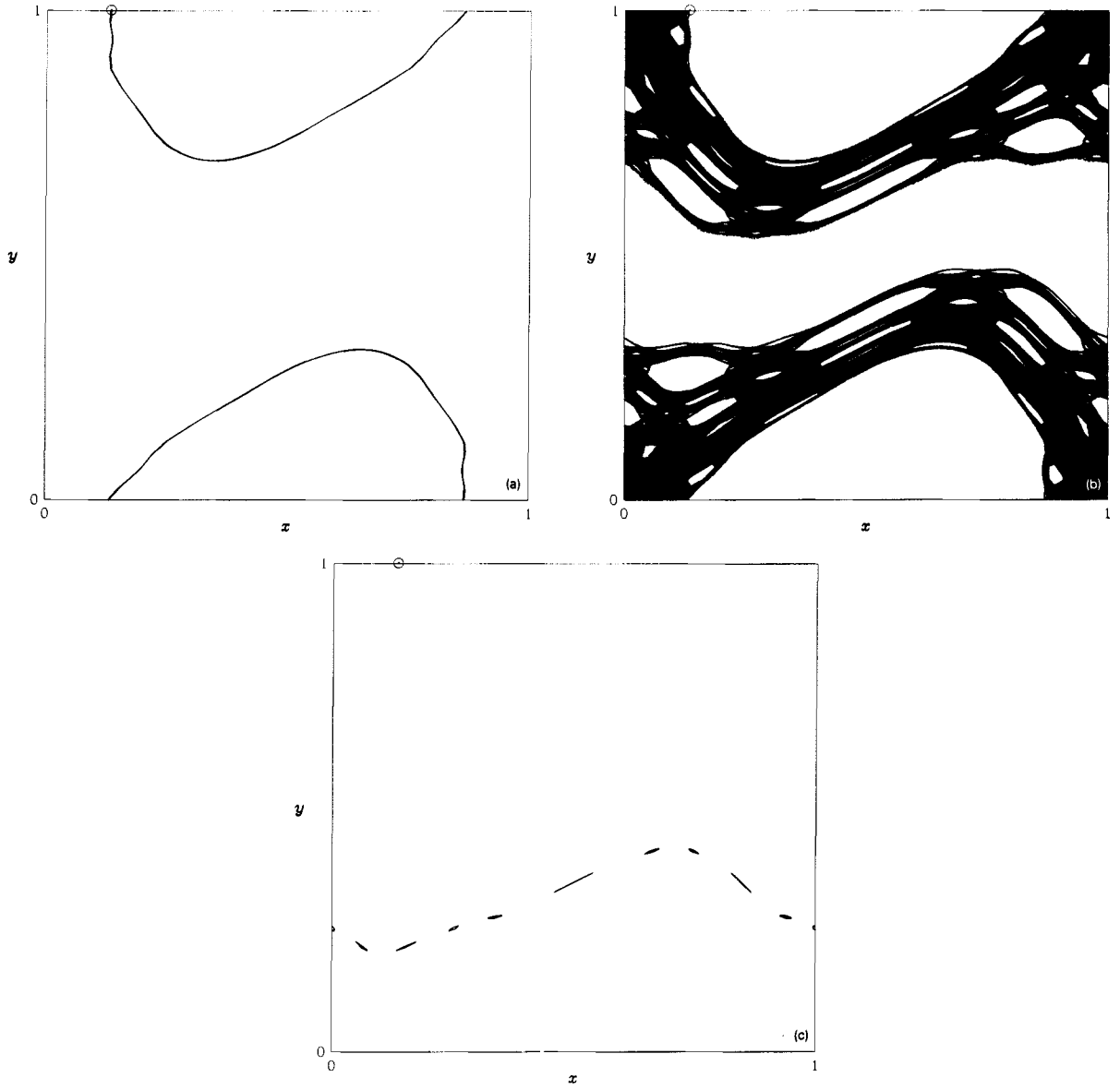

Fig. 8. An example of unsatisfactory behaviour of the floating-point map R_4 with $K = 1$. The initial point of this trajectory is $(x, y) = (0.133, 1.0)$. (a) The first 40 000 iterations display an apparently regular trajectory. (b) The next 1 730 000 iterations show an apparently chaotic orbit. The limit circuit is reached near the end of this interval. (c) The limit circuit has length only 37 310 iterations and appears to be a regular orbit (a chain of islands).

arithmetic can, in principle, corrupt these calculations in a serious way. In a floating-point map, roundoff can (i) unnaturally shift a trajectory from a region dominated by regular orbits into a region dominated by chaotic orbits or vice versa, and (ii) prevent cyclic, qualitative changes that ought to occur. These problems should not occur in lattice maps.

Problem (ii) is illustrated in fig. 8. The floating-point map R_4 with $K = 1$ is iterated from $(x, y) = (0.133, 1.0)$. The trajectory appears to be regular for the first 40 000 iterations (fig. 8a). It

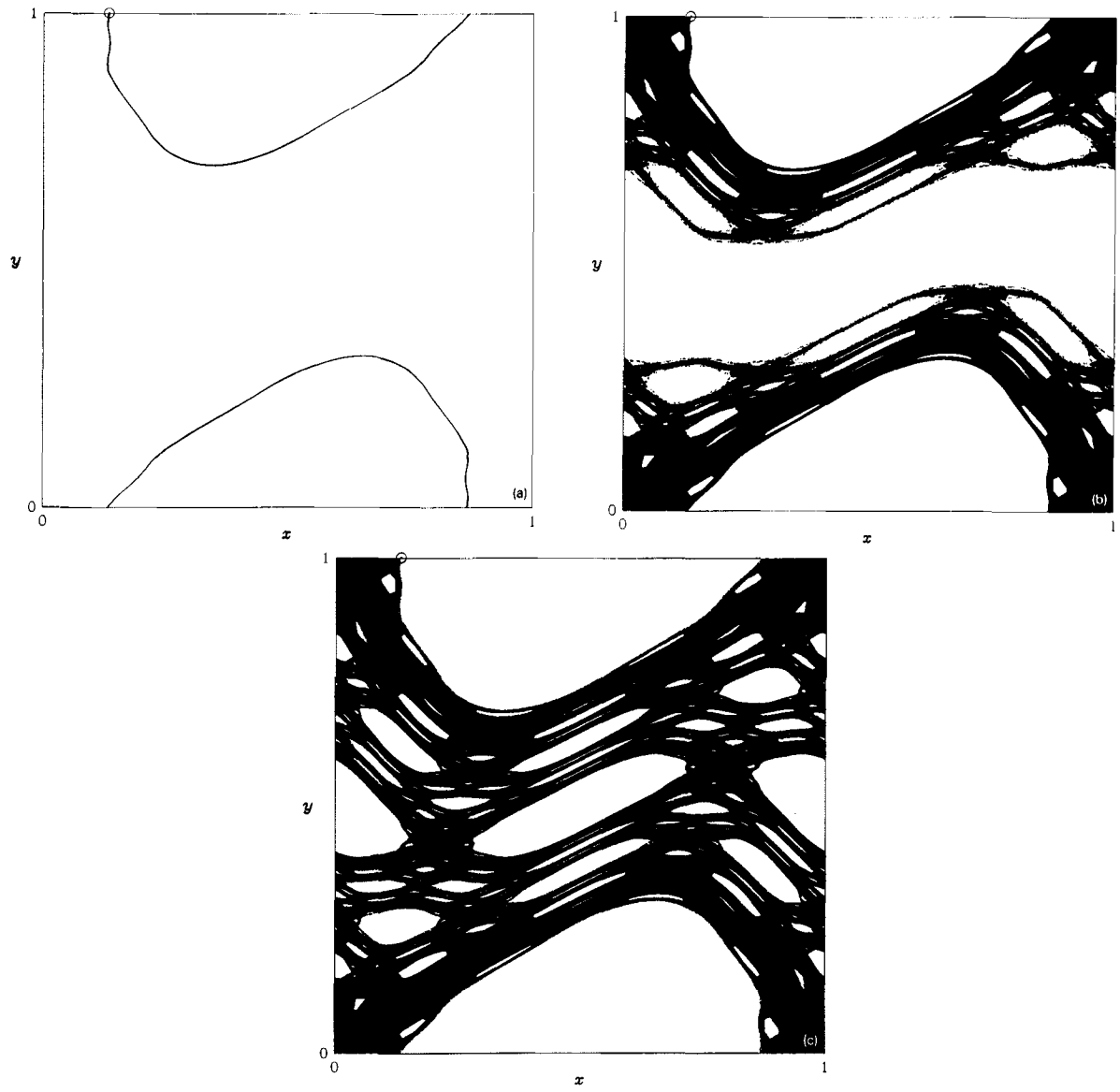

Fig. 9. Complete orbits of the mappings I_m started from the same point as in the plots in fig. 8. (a) $m = 10^5$, cycle length $L = 13582$. (b) $m = 10^6$, $L = 552378$. (c) $m = 10^9$; the trajectory was stopped after 10^7 iterations.

then appears to slip into the chaotic region and travels through most of it until reaching the limit circuit after 1 734 198 iterations (fig. 8b). The limit circuit appears to be regular (it is a chain of islands) and has length only 37 310 iterations (fig. 8c).

The results of lattice maps applied to the same initial point used for fig. 8 are shown in fig. 9. We have selected $\mathrm{traj}_{I_m}((0.133m, m))$ for $m = 10^5$, 10^6, and 10^9 because these show the three types of orbits that we have found by examining many values of m. The orbit either appears regular (fig. 9a), is chaotic but does not fill the chaotic region of the phase plane (fig. 9b), or does fill the whole chaotic region (fig. 9c).

The plots of $\mathrm{traj}_{I_m}((0.133m, m))$ look very different for different values of m because the initial point is near the "chaos boundary" (the boundary

between the regular region and the "chaotic sea") and the exact location of that boundary differs for different values of m. It is known [16] that if such chaos boundaries exist then most chaotic orbits alternate between long periods of chaotic behaviour and short periods of regular behaviour, due to "trapping" near the chaos boundaries. The advantage of the lattice maps over the floating-point map is that a chaotic trajectory is never artificially trapped permanently on a short regular orbit.

To illustrate the behaviour of the floating-point map R_4 in more detail, we now describe the complete evolution of all the trajectories of the lattice map that are shown in fig. 1 (see table 1). None of these 37 trajectories of R_4 (with $K = 1$) begins on a limit circuit. Some of the trajectories that appear to be chaotic for long times have short, apparently regular limit circuits; others have long and apparently chaotic limit circuits. All the long limit circuits have the same length; in fact, they are all the identical circuit (we checked this by comparison against a particular point). This long limit circuit appears to cover the entire chaotic region. Trajectories 33 and 37 in table 1 have chaotic transients that lead to the same short limit circuit, which is a chain of islands.

The convergence of several of the orbits to the same limit circuit, and the relatively short length of this circuit, are striking in view of the large number of representable points available to the map in the unit square, $M = (2^7 \cdot 2^{23})^2 \simeq 1.15 \times 10^{18}$. The average length, $\langle L \rangle$, of a chaotic limit circuit can be estimated using random map theory [2, 17] to be $\langle L \rangle \sim \sqrt{M} \sim 10^9$. Since the representable points are not uniformly distributed in the plane ($(\frac{15}{16})^2 \simeq 88\%$ of the unit square contains only $(1/2^{7-3})^2 = (\frac{1}{16})^2 \simeq 0.4\%$ of the representable points) it is perhaps more reasonable to estimate $\langle L \rangle \sim \sqrt{(2^3 \cdot 2^{33})^2} = 2^{26} \simeq 6.7 \times 10^7$. We expect $\langle L \rangle$ to be smaller still due to the symmetries of the standard map [24]. All this takes away the surprise in the length of the longest limit circuit observed. Experience with other maps suggests that the longest limit circuit will tend to attract most of the orbits (see ref. [6] and references therein).

Table 1
Data for a small sample of trajectories of R_4 with $K = 1$. The first 2000 points of all these trajectories are plotted in fig. 1.

	x_0	y_0	Transient	Limit circuit	Total length
1	0.15	1.00	1788604	13256	1801860
2	0.17	1.00	52860	17521	70381
3	0.19	1.00	195848	41536	237384
4	0.20	1.00	112552	9760	122312
5	0.24	1.00	44509	403	44912
6	0.26	1.00	2148397	1622	2150019
7	0.28	1.00	179221	2434	181655
8	0.30	1.00	164489	33521	198010
9	0.33	1.00	15394	19555	34949
10	0.35	1.00	166084	1104	167188
11	0.38	1.00	271903	1825	273728
12	0.40	1.00	102822	827	103649
13	0.43	1.00	241968	2058	244026
14	0.45	1.00	25029	52843	77872
15	0.10	0.80	2884840	6123	2890963
16	0.01	0.80	49049	20780	69829
17	0.99	0.20	61235	12200	73435
18	0.01	0.78	12534871	10458863	22993734
19	0.99	0.22	12006160	10458863	22465023
20	0.01	0.61	4055799	10458863	14514662
21	0.99	0.39	8587216	10458863	19046079
22	0.12	0.62	103568	4884	108452
23	0.88	0.38	272839	2172	275011
24	0.19	0.58	195953	3552	199505
25	0.81	0.42	1417518	2127	1419645
26	0.01	0.59	28436	9780	38216
27	0.01	0.55	66421	146	66567
28	0.01	0.52	340099	490	340589
29	0.10	0.50	317147	2008	319155
30	0.23	0.50	110662	1620	112282
31	0.77	0.50	17141	6015	23156
32	0.10	0.70	8281074	10458863	18739937
33	0.90	0.30	6300097	54264	6354361
34	0.10	0.30	9888	38203	48091
35	0.90	0.70	85394	2838	88232
36	0.10	0.20	9897940	10458863	20356803
37	0.90	0.80	1179489	54264	1233753

Our experiments encourage us to view the limit circuits of floating-point maps as attractors, the existence of which is one of the main characteristics of *dissipative* dynamical systems. (The major difference is that very similar transients can be attracted to very different limit circuits; thus the basin of attraction of a limit circuit may be very

complicated.) We have avoided the terms "limit cycle", commonly used for periodic attractors, and "strange attractor", used for chaotic attractors, because limit circuits are always periodic but can be either regular or chaotic.

Of course, if the trajectories were followed using `REAL*8` rather than `REAL*4` arithmetic, as is usual in numerical studies, the roundoff errors would be much smaller, and both the transients and the limit circuits would be much longer. However, the qualitative behaviour of the orbits would be the same. The reasons we used `REAL*4` arithmetic are: (i) so that the effects of roundoff would show up more quickly; (ii) our lattice maps use `INTEGER*4` arithmetic and it is fair to compare the behaviour of floating-point and integer maps using the same storage per number (four bytes).

Our central point is that because the lattice maps are themselves Hamiltonian maps, they are better representations of real Hamiltonian dynamical systems than can be obtained using floating-point arithmetic. They can never display "forbidden" behaviour such as crossing invariant curves and attraction to limit circuits. I_{10^6} is considerably more successful than R_4 in modeling the long-term behaviour of the standard map, even though the former employs fewer "digits of accuracy" (`REAL*4` has a precision of seven decimal digits). Even for small m it is impossible for I_m to display non-Hamiltonian behaviour. Thus we find considerable advantage in avoiding roundoff error in this way.

4. Transition to global stochasticity

For the standard map, there is a critical value of the stochasticity parameter such that if $K < K_{\text{crit}}$ then chaotic motion is restricted to a limited range in y (or Y) bounded by KAM curves, while if $K > K_{\text{crit}}$ chaotic orbits can wander over the entire range of y (no KAM curves spanning the whole x coordinate exist). In the latter case, the map is said to be globally stochastic. The critical value marking the transition to global stochasticity is found to be $K_{\text{crit}} \simeq 0.97$ (e.g., ref. [20] §4.7).

There is a simple way to test for global stochasticity in the lattice map. Consider trajectories of I_m (*not* modulo m) with initial states on the portion of the lattice in the central square, i.e., such that $X_0, Y_0 \in \{0, 1, \ldots, m-1\}$ (it is sufficient to consider these initial states since the map is spatially periodic with period m). If we follow such a trajectory with I_m, eventually it must either (i) return to the point (X_0, Y_0), or (ii) reach the point $(X_0 + km, Y_0)$ where $k \neq 0$ is an integer, or (iii) reach the point $(X_0 + km, Y_0 + lm)$ where k and l are integers, $l \neq 0$. In case (i) or (ii) the orbit is not globally stochastic since the excursions in Y are finite, while in case (iii) it is globally stochastic since Y must increase or decrease without limit. In practice, we test for global stochasticity in the lattice map I_m by considering $X \pmod m$ and Y (*not* $\bmod m$), and we iterate until iteration number N where $(X_N, Y_N) = (X_0, Y_0 + lm)$ or until $|Y_j - Y_0| > 2m$, whichever happens first. The orbit is globally stochastic if and only if $l \neq 0$; in the latter instance we know $|l| > 2$ so this is sufficient. (No invariant curves can stretch over more than a range of $2m$ in Y (R.S. MacKay, private communication). This follows from a theorem of Birkhoff [21].)

In this section, we discuss numerical experiments that show that a transition to global stochasticity occurs in I_m, and that as m is increased K_{crit} approaches 0.97. It is interesting to see that this important feature of the standard map is successfully reproduced by our lattice maps.

Since I_m is restricted to a lattice, it is possible in principle to iterate *all* the orbits starting in the central square and determine if any are globally stochastic. However, for large m this search is too computationally expensive, so for $m \gtrsim$ a few hundred we must restrict our attention to a sample of orbits.

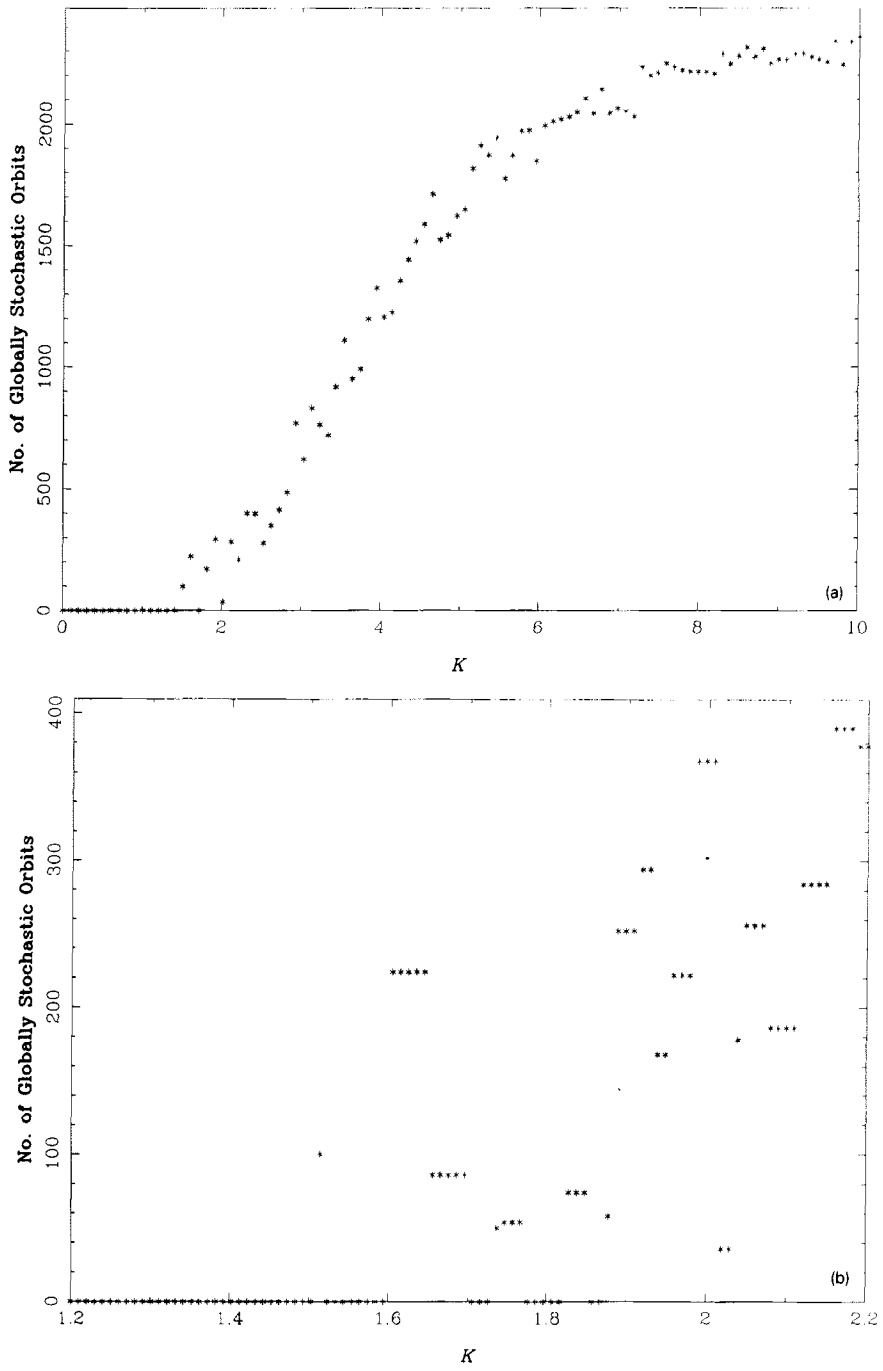

Fig. 10. The number of globally stochastic orbits as a function of the stochasticity parameter K, for $m = 50$. The results of narrow-range experiments (b) were used to obtain the values in table 2, which are plotted in fig. 11.

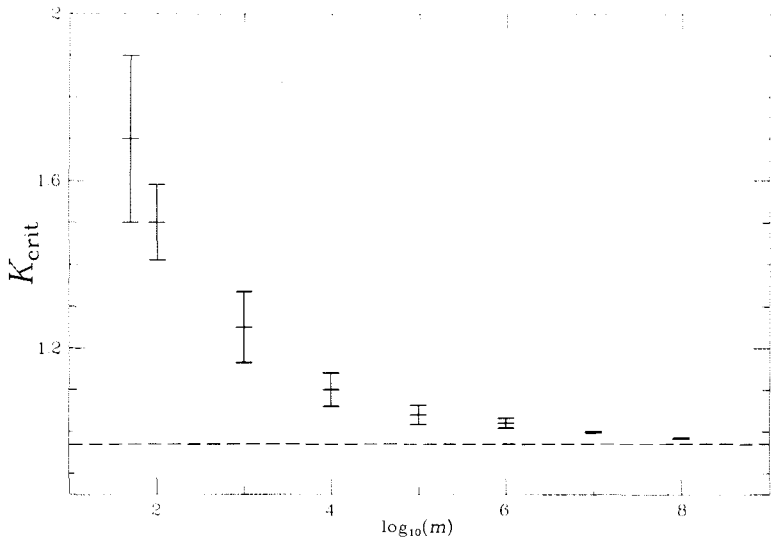

Fig. 11. The relationship between m and K_{crit} (see section 3). The plotted points are listed in table 2. The dashed line shows the best estimate obtained for the standard map by other methods, $K_{crit} = 0.97$.

For a sequence of 100 values of K ($0 \leq K \leq 10$) we have examined all central square initial states of I_{50}, and noted the number of globally stochastic orbits for each K. The results are plotted in fig. 10a. From this figure we selected a smaller range of K ($1.2 \leq K \leq 2.2$) for a second sequence of 100 values (fig. 10b). We define K_{crit} for I_{50} to be the midpoint between the smallest value of K (in fig. 10b) for which globally stochastic orbits occur and the largest value of K for which there are no globally stochastic orbits. (This value is the first entry in table 2, and the first point plotted in fig. 11.)

For $m = 100$ we have also evolved all central square initial states and arrived at a value for K_{crit} as we did for $m = 50$. Still considering sequences of 100 values of K, we have evolved a smaller, carefully chosen 10^2 grid of initial states of I_m for $m = 10^3$, 10^4 and 10^5. (The grid was chosen in $[0, \frac{1}{10}]^2$ where all the orbits are chaotic.)

For $m = 10^6$ we have considered only a 5^2 grid in $[0, \frac{1}{10}]^2$, but we still checked 100 values of K. For $m = 10^7$ and 10^8 we have considered a 3^2 grid and 10 values of K.

Table 2
The critical value of the stochasticity parameter for the lattice map I_m. The meaning of the errors is discussed in section 3. See figs. 10 and 11.

m	K_{crit}	Error
50	1.7	0.2
10^2	1.5	0.09
10^3	1.25	0.085
10^4	1.10	0.04
10^5	1.04	0.023
10^6	1.02	0.012
10^7	0.998	0.002
10^8	0.9833	0.0011

All our results are summarized in table 2 and fig. 11. The errors show the interval from which K_{crit} was chosen as the midpoint, as described above. The horizontal dashed line in fig. 11 is at $K_{crit} = 0.97$, the "best value" predicted for the standard map by other methods (see ref. [20], chapter 4). For large m, the lattice map yields a value of K_{crit} that agrees to within 1% with this value.

5. A lattice map with three degrees of freedom

Chaotic trajectories of Hamiltonian systems with $N \geq 3$ degrees of freedom are not confined between invariant tori (invariant tori have dimension at most N while constant energy manifolds have dimension $2N-1$). This permits a kind of wandering of chaotic trajectories known as Arnol'd diffusion (e.g., ref. [20], chapter 6). It is generally believed that this process leads generic chaotic trajectories arbitrarily close to every point in phase space.

The timescale for Arnol'd diffusion is generally very long, so it is difficult to observe Arnol'd diffusion numerically. If the calculations use floating-point arithmetic, there is also some diffusion due to roundoff error and it may be difficult to distinguish Arnol'd diffusion from this numerical diffusion. Diffusion of either sort will stop abruptly when a trajectory's limit circuit is reached. The success of a map in modeling a real Hamiltonian system over very long times could depend strongly on the structure of this "attractor".

Since mappings of dimension greater than 2 cannot easily be represented on a plane, interpretation of results is much more difficult. Moreover, the set of representable points in a space of dimension greater than 2 is far larger than the set of representable points in the plane. Thus maps of dimension greater than 2 generally have very long limit circuits and the sorts of experiments we have described in the previous section would be very expensive for such systems. This is why we have used the standard map to illustrate the problems with roundoff error and the advantages of lattice maps. We now discuss a limited set of experiments using a lattice map to study Arnol'd diffusion in a Hamiltonian system with three degrees of freedom.

Tennyson et al. [27] (see also ref. [20], §6.1b) study Arnol'd diffusion in a four-dimensional symplectic mapping[#5] that corresponds to a surface of section of a three-dimensional billiards problem. The map can be written

$$\begin{aligned}
a_{n+1} &= a_n - \frac{\alpha_x k_x}{\pi}\sin 2\pi k_x x_n \\
&\quad + \frac{\mu k_x}{2\pi}\sin 2\pi(k_x x_n + k_y y_n), \\
x_{n+1} &= x_n + \frac{h}{\pi}\tan 2\pi a_{n+1}, \\
b_{n+1} &= b_n - \frac{\alpha_y k_y}{\pi}\sin 2\pi k_y y_n \\
&\quad + \frac{\mu k_y}{2\pi}\sin 2\pi(k_x x_n + k_y y_n), \\
y_{n+1} &= y_n + \frac{h}{\pi}\tan 2\pi b_{n+1}. \qquad (7)
\end{aligned}$$

As in the case of the standard map, we change coordinates to $A = ma$, $X = mx$, $B = mb$, $Y = my$, and replace the non-linear functions by lattice invariant functions defined on the lattice by

$$\begin{aligned}
S_{m,\alpha,k}(X) &= \left[\frac{m\alpha k}{\pi}\sin\frac{2\pi kX}{m}\right], \\
G_{m,k}(X,Y) &= \left[\frac{m\mu k}{2\pi}\sin\frac{2\pi}{m}(k_x X_n + k_y Y_n)\right], \\
T_m(A) &= \left[\frac{mh}{\pi}\tan\frac{2\pi A}{m}\right]. \qquad (8)
\end{aligned}$$

(Note that since the tangent function is unbounded, there are always values of A for which evaluation of $T_m(A)$ causes integer overflow in the computer. However, this turns out not to be a concern in practice for the experiments we have done.) The map that we iterate exactly on the computer is

$$\begin{aligned}
A_{n+1} &= A_n - S_{m,\alpha_x,k_x}(X_n) + G_{m,k_x}(X_n, Y_n), \\
X_{n+1} &= X_n + T_m(A_{n+1}), \\
B_{n+1} &= B_n - S_{m,\alpha_y,k_y}(Y_n) + G_{m,k_y}(X_n, Y_n), \\
Y_{n+1} &= Y_n + T_m(B_{n+1}), \qquad (9)
\end{aligned}$$

where capital letters denote integers or integer functions. This map (9) is one-to-one, and it can

[#5] Diffusion in a four-dimensional mapping was studied earlier by Froeschlé [10, 11]. See also ref. [12].

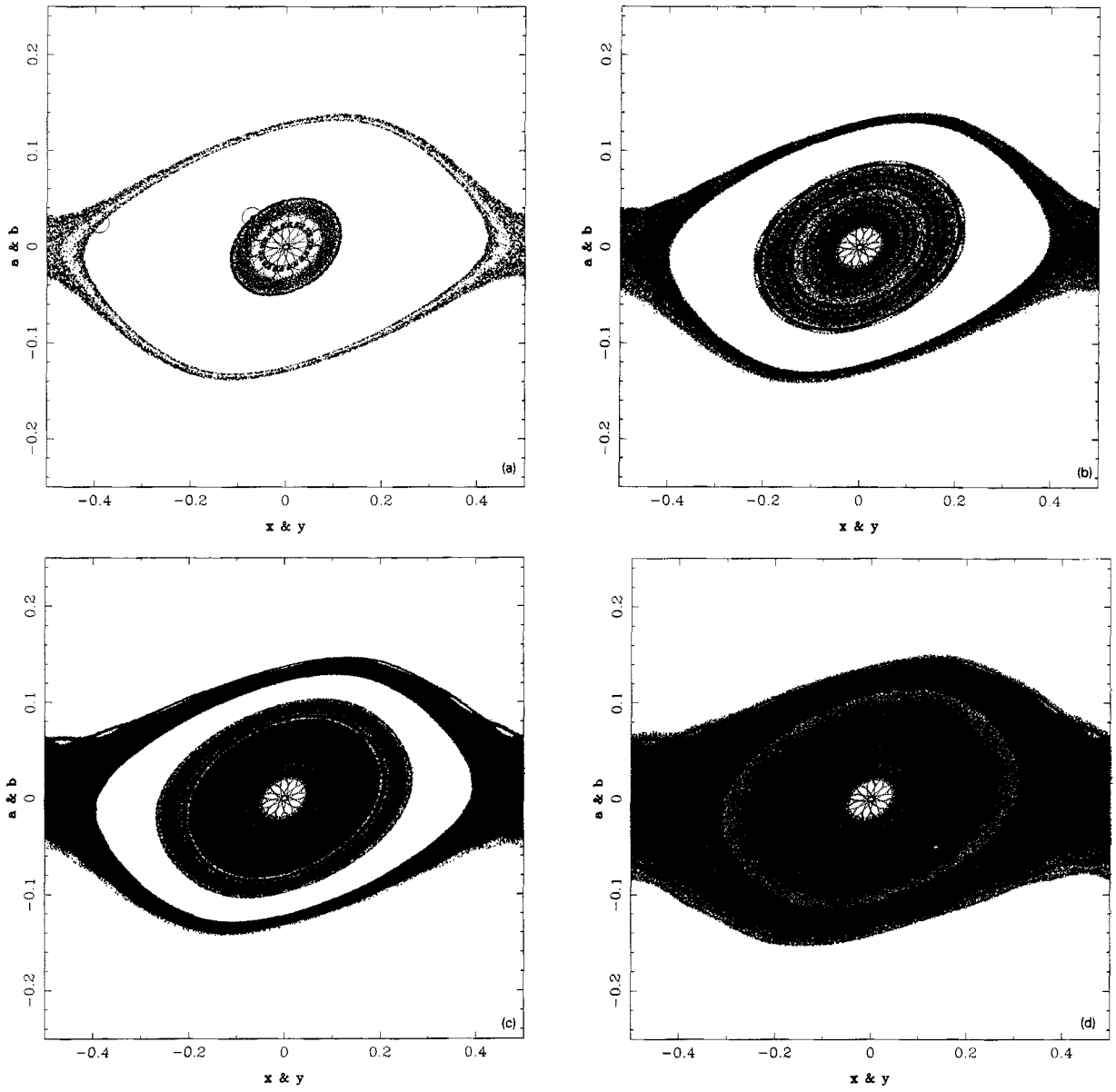

Fig. 12. The lattice map (9) with $m = 10^9$. This map is derived from the map (7) of Tennyson et al. [27]. The parameter values are as discussed in section 4. The initial point is $(x_0, a_0, y_0, b_0) = (-0.07, 0.03, -0.391, 0.25)$. (a) $N = 10^4$ iterations. (b) $N = 10^5$. (c) $N = 5 \times 10^5$. (d) $N = 8 \times 10^5$. The plots show motion both in the x–a plane (inner points) and in the y–b plane (outer points).

be extended to a symplectic diffeomorphism on the whole phase space (see section 5).

In order to study the four-dimensional surface of section with coordinates (x, a, y, b) Tennyson et al. plot two points (x, a) and (y, b) on a plane at each iteration of the map. We have done the same using the lattice map (9). Tennyson et al. focus attention on parameters chosen with the constraints $\lambda_x : h : \alpha_x$ and $\lambda_y : h : \alpha_y$ as $100 : 10 : 2$ (where $\lambda_i = 2\pi/k_i$) and $\mu/h = 0.004$. With these restrictions there is only one free parameter in the map. We took this to be $k \equiv k_x = k_y$.

Following Tennyson et al., we choose an initial state that is on an island encircling the central

resonance in x–a space and within the thin separatrix stochastic layer in y–b space. Arnol'd diffusion is revealed if motion in x–a space is not restricted to the island on which the trajectory starts, but covers a finite area and eventually explores the entire plane.

In fig. 12 we show results of iterating the lattice map (9) with $m = 10^9$ from the initial point $(x_0, a_0, y_0, b_0) = (-0.07, 0.03, -0.391, 0.25)$. These plots should be compared with fig. 16 in Tennyson et al. or fig. 6.6 in ref. [20]. Our lattice map roughly reproduces the results of Tennyson et al., in that the trajectory slowly diffuses over most of the x–a plane, so it is reasonable to conclude that the diffusion they observe is not the result of roundoff error. We do, however, seem to find a faster rate of diffusion and this is not sensitive to the value of m if $m \gtrsim 10^4$; the lattice map trajectories explore more of the plane after 10^6 iterations than the Tennyson et al. trajectory explores in 10^7 iterations. Of course, the significance of this difference is difficult to assess, since the diffusion rate of a given orbit may be very sensitive to the initial conditions and to other details of the calculation.

The parameter μ in (7) determines the amount of coupling between the x and y motions of the bouncing billiard ball. If $\mu = 0$ then there is no coupling and no Arnol'd diffusion. For any $\mu > 0$ there should be Arnol'd diffusion but for small enough μ in the map (7) the coupling will not be resolved by the lattice map (9). The limiting value of μ can easily be estimated. If

$$g = \frac{m\mu k}{2\pi} \sin \frac{2\pi}{m}(k_x X_n + k_y Y_n),$$

then in the notation of (8) and (9) $G = [g]$. If $G \neq 0$ then we must have $|g| \geq \frac{1}{2}$. Therefore, if we want most of the coupling to be resolved by the map then we require

$$1 \lesssim \langle g^2 \rangle^{1/2} = \frac{m\mu k}{2\pi} \langle \sin^2 \theta \rangle^{1/2} = \frac{m\mu k}{2\sqrt{2}\,\pi}, \quad \text{i.e.,}$$

$$m\mu \gtrsim \frac{2\sqrt{2}\,\pi}{k} \approx \frac{10}{k}, \tag{10}$$

where angle brackets denote average. With the parameter relations discussed above, $k = 1$ implies $\mu = 0.0025$ so (10) indicates that we require $m \gtrsim 4000$ in order to see Arnol'd diffusion, consistent with our numerical experiments that show that diffusion sets in between $m = 10^3$ and $m = 10^4$. Note that $m\mu$ is roughly the ratio of magnitudes of kicks due to coupling ($\sim \mu$) to kicks due to discretization ($\sim 1/m$). For floating-point arithmetic, kicks due to discretization are of order the numerical precision, $\approx 10^{-7}$ for `REAL*4`; thus with $\mu = 0.0025$ the roundoff error is not likely to overshadow the Arnol'd diffusion. In a system that is not designed to display Arnol'd diffusion like the present one, such estimates are bound to be much more difficult. By using a lattice map rather than a floating-point map we ensure that roundoff does not force any non-Hamiltonian diffusion on the system.

5. Lattice maps in general

The two maps we have considered are in the general form

$$\boldsymbol{\Theta}_{n+1} = \boldsymbol{\Theta}_n + \boldsymbol{A}(\boldsymbol{J}_{n+1}),$$

$$\boldsymbol{J}_{n+1} = \boldsymbol{J}_n + \boldsymbol{B}(\boldsymbol{\Theta}_n), \tag{11}$$

where $\boldsymbol{\Theta}$ and $\boldsymbol{J}$ are N-vectors, $\boldsymbol{A}$ and $\boldsymbol{B}$ are differentiable N-vector valued functions, and $2N$ is the dimension of the map. Setting $(\boldsymbol{\Theta}_{k+1}, \boldsymbol{J}_{k+1}) = (\boldsymbol{\Theta}_{l+1}, \boldsymbol{J}_{l+1})$ we find $(\boldsymbol{\Theta}_k, \boldsymbol{J}_k) = (\boldsymbol{\Theta}_l, \boldsymbol{J}_l)$ so the map is one-to-one. This result does not depend at all on the forms of the functions $\boldsymbol{A}$ and $\boldsymbol{B}$ so when we replace $\boldsymbol{A}$ and $\boldsymbol{B}$ by lattice invariant functions the new map is also automatically one-to-one. This is the most basic property of Hamiltonian maps ("phase trajectories do not intersect"). It does not hold for floating-point versions of (11) because normal addition is then replaced by floating-point addition (see Ap-

pendix). Since the map is one-to-one even if $\boldsymbol{A}$ and $\boldsymbol{B}$ are not one-to-one, roundoff error is only important for the additions in (11).

The map (11), which we call T, can be written as a composition, $T = S_2 \circ S_1$, of the two "shears"

$$S_1\begin{pmatrix}\boldsymbol{\Theta}\\ \boldsymbol{J}\end{pmatrix} = \begin{pmatrix}\boldsymbol{\Theta}\\ \boldsymbol{J}+\boldsymbol{B}(\boldsymbol{\Theta})\end{pmatrix}, \quad S_2\begin{pmatrix}\boldsymbol{\Theta}\\ \boldsymbol{J}\end{pmatrix} = \begin{pmatrix}\boldsymbol{\Theta}+\boldsymbol{A}(\boldsymbol{J})\\ \boldsymbol{J}\end{pmatrix}. \tag{12}$$

It is easily seen that a shear is both one-to-one and onto, and its (global) inverse can be written explicitly. For example,

$$S_1^{-1}\begin{pmatrix}\boldsymbol{\Theta}\\ \boldsymbol{J}\end{pmatrix} = \begin{pmatrix}\boldsymbol{\Theta}\\ \boldsymbol{J}-\boldsymbol{B}(\boldsymbol{\Theta})\end{pmatrix}.$$

Thus a differentiable shear is a (global) diffeomorphism (e.g., S_1 is a diffeomorphism provided $\boldsymbol{B}$ is differentiable, which is the situation of interest here). It follows that a composition of differentiable shears, such as T, is a diffeomorphism.

As a result of the decomposition, $T = \boldsymbol{S}_2 \circ \boldsymbol{S}_1$, the Jacobian matrix T' of T can be written as a block matrix that factors conveniently,

$$T' = \begin{pmatrix}\mathbf{I}+\boldsymbol{A}'\boldsymbol{B}' & \boldsymbol{A}'\\ \boldsymbol{B}' & \mathbf{I}\end{pmatrix} = \begin{pmatrix}\mathbf{I} & \boldsymbol{A}'\\ \mathbf{0} & \mathbf{I}\end{pmatrix}\begin{pmatrix}\mathbf{I} & \mathbf{0}\\ \boldsymbol{B}' & \mathbf{I}\end{pmatrix} = S_2'S_1'. \tag{13}$$

$\mathbf{I}$ and $\mathbf{0}$ denote the N-dimensional unit and zero matrices, and $\boldsymbol{A}'$ and $\boldsymbol{B}'$ denote the Jacobian matrices of $\boldsymbol{A}$ and $\boldsymbol{B}$, respectively. The factorization (13) makes it clear that the determinant of T' is unity, so T is volume-preserving. Again, this result does not depend on the functional forms of $\boldsymbol{A}$ and $\boldsymbol{B}$ (provided, of course, that they are differentiable). It follows that our lattice map approximation of T can always be extended to a volume-preserving diffeomorphism on the whole phase space. In particular, this shows that the lattice map I_m derived from the standard map can be extended to an area-preserving diffeomorphism on $\mathbb{R}^2$.

The only property of a symplectic diffeomorphism that converts directly into a property of a map on a discrete set is that of being a one-to-one correspondence. We define a map on a lattice to be Hamiltonian if it is one-to-one and can be extended to a symplectic diffeomorphism on the differentiable manifold on which the original map is defined; this ensures that the map that we iterate exactly is Hamiltonian is precisely the same sense as the original map. We show now that if the original map (11) is Hamiltonian then our induced lattice map is Hamiltonian and "close" to the original map. This shows, in particular, that the four-dimensional integer map studied in section 4 is Hamiltonian and "close" to the map of Tennyson et al. [27].

Theorem. If the original map T (11) is symplectic then the lattice map induced on the lattice L_m of spacing $1/m$ is the restriction to L_m of a symplectic diffeomorphism $\tilde{T}$ on $\mathbb{R}^{2N}$ that differs from the original map by at most $\sqrt{N/2}\,/m$ at any point.

Proof. A map is symplectic if and only if it is differentiable and its Jacobian M is a symplectic matrix, i.e., $M^{\mathrm{T}}JM = J$, where $J = \begin{pmatrix}\mathbf{0} & \mathbf{I}\\ -\mathbf{I} & \mathbf{0}\end{pmatrix}$. A composition of symplectic maps is symplectic. Hence, since we have shown above that a composition of differentiable shears is a diffeomorphism, it is sufficient to show that the lattice map derived from a symplectic shear can itself be extended to a symplectic shear.

Let $\boldsymbol{x}^l$, $l = 1, 2, \ldots$, denote the lattice points in $\mathbb{R}^N$, and let $[\boldsymbol{x}]$ denote the lattice point nearest to $\boldsymbol{x}$. Let S denote an arbitrary differentiable shear and let $\boldsymbol{C}$ denote the "shearing function" (e.g., for $S = S_1$, $\boldsymbol{C} = \boldsymbol{B}$). The shear S is symplectic if and only if $\boldsymbol{C}'$ is symmetric. The lattice map derived from S can be extended to a symplectic shear $\tilde{S}$ provided there is a differentiable function $\tilde{\boldsymbol{C}}$ such that $\tilde{\boldsymbol{C}}'$ is symmetric and $\tilde{\boldsymbol{C}}(\boldsymbol{x}^l) = [\boldsymbol{C}(\boldsymbol{x}^l)]$, for all l. To obtain the required bound on the difference between the original and new maps

we also require $\|\tilde{\boldsymbol{C}}(\boldsymbol{x}) - \boldsymbol{C}(\boldsymbol{x})\| \le \sqrt{N}/2m$, for all $\boldsymbol{x}$. Provided the original shear S is symplectic (i.e., $\boldsymbol{C}'$ is symmetric) such a function $\tilde{\boldsymbol{C}}$ can be constructed as follows.

Let f^l be a twice continuously differentiable scalar function such that

(i) $f^l(\boldsymbol{x}^l) = 0$,

(ii) $f^l(\boldsymbol{x}) = 0$ if $\|\boldsymbol{x} - \boldsymbol{x}^l\| \ge \frac{1}{2m}$,

(iii) $\frac{\partial f^l}{\partial \boldsymbol{x}}(\boldsymbol{x}^l) = \left[\boldsymbol{C}(\boldsymbol{x}^l)\right] - \boldsymbol{C}(\boldsymbol{x}^l)$.

Since $\|[\boldsymbol{C}(\boldsymbol{x}^l)] - \boldsymbol{C}(\boldsymbol{x}^l)\| \le \sqrt{N}/2m$ (the distance from the centre of an N-cube of side $1/m$ to one of its corners), f^l can also be chosen such that

(iv) $\left\| \frac{\partial f^l}{\partial \boldsymbol{x}}(\boldsymbol{x}) \right\| \le \frac{\sqrt{N}}{2m}$, for all $\boldsymbol{x}$.

Now let

$$\tilde{\boldsymbol{C}}(\boldsymbol{x}) \equiv \boldsymbol{C}(\boldsymbol{x}) + \sum_l \frac{\partial f^l}{\partial \boldsymbol{x}}.$$

This function $\tilde{\boldsymbol{C}}$ has all the required properties. Hence, the desired new map $\tilde{T}$ can be obtained by replacing $\boldsymbol{A}$ and $\boldsymbol{B}$ in T with $\tilde{\boldsymbol{A}}$ and $\tilde{\boldsymbol{B}}$. For the full map, we obtain the bound $\|\tilde{T} - T\| \le \sqrt{2N}/2m = \sqrt{N/2}/m$. This completes the proof. □

Many interesting Hamiltonian maps can be put in the form (11). For any such system our lattice map method is directly applicable without modification, i.e., the construction of a Hamiltonian lattice map is trivial. In general, due to a theorem of Lax [18], it is possible to replace any continuous measure-preserving map by a good[#6] approximation that is a permutation of a given lattice. Symplectic maps preserve phase space volume, so Lax's theorem shows that symplectic maps can always be approximated well by a permutation of a given lattice. Unfortunately, there is no fast algorithm known to construct Lax's good lattice permutation (it is also not clear that such a permutation can always be extended to a symplectic diffeomorphism). Thus the usefulness of lattice maps may be limited to a subset of Hamiltonian systems.

Lattice maps can be used to find exactly Hamiltonian numerical approximations to Hamiltonian flows. As a simple illustration, we note that the standard "leapfrog" numerical integration scheme for Hamiltonians in the form $H = \frac{1}{2}\boldsymbol{v}^2 + U(\boldsymbol{x})$,

$$\boldsymbol{x}(t + \Delta t) = \boldsymbol{x}(t) + \Delta t\, \boldsymbol{v}(t + \Delta t),$$

$$\boldsymbol{v}(t + \Delta t) = \boldsymbol{v}(t) - \Delta t \frac{\partial U}{\partial \boldsymbol{x}}(\boldsymbol{x}(t)),$$

has the form of the map (11) with $\boldsymbol{A}$ the identity function (define $\boldsymbol{x}_n \equiv \boldsymbol{x}(n\,\Delta t)$, $\boldsymbol{v}_n \equiv \boldsymbol{v}(n\,\Delta t)$ and choose units so that $\Delta t = 1$). For any continuously differentiable U, the Jacobian matrix of $\partial U/\partial \boldsymbol{x}$ is symmetric, so "integerized leapfrog" is exactly symplectic.

The use of lattice maps to construct exactly symplectic integration algorithms of any order for general Hamiltonians is discussed in a forthcoming paper by Scovel [25].

6. Shadowing trajectories

Roughly speaking, an approximate trajectory is said to be "shadowed" by a true trajectory of a given map if the true trajectory starts near the initial point of the approximate trajectory and remains close to it for many iterations. The main purpose of shadowing theorems is to show rigorously that apparently chaotic trajectories computed numerically are shadowed by true trajectories of the system under study.

In a recent paper Grebogi et al. [14] discuss the meaning and relevance of shadowing theorems and give some shadowing results for the standard map.

[#6] The approximation F_m of F on the lattice L_m of spacing $1/m$ is "good" if, given a lattice point p and the cube C_p of side-length $1/m$ centered on p, $F(C_p)$ has a point in common with the cube of side-length $1/m$ centered on $F_m(p)$.

Grebogi et al. use a computer-based proof to establish shadowing. Unfortunately, the method is only applicable to individual trajectories, one at a time, and it is more computationally expensive to prove that a given numerical trajectory is shadowed by a true trajectory than it is to compute the numerical trajectory. This limits the practical value of the method, but experience leads Grebogi et al. to conjecture a useful rule of thumb for a two-dimensional Hamiltonian map: if the typical error per step in a numerical trajectory is $\delta > 0$, then a true trajectory shadows the numerical trajectory with error $\sim \sqrt{\delta}$ for $\sim 1/\sqrt{\delta}$ iterations. Applying this to our lattice maps I_m we estimate that for a given trajectory of I_m there are trajectories of the standard map that stay within a distance $1/\sqrt{m}$ of the trajectory of I_m for approximately $\sqrt{m}$ iterations. We have iterated trajectories for much longer than this timescale so we feel obliged to justify our results in this context.

Trajectories of a floating-point map represent orbits of a Hamiltonian system only for as many iterations as they are shadowed by trajectories of an exact Hamiltonian map. Our lattice maps do not suffer from this limitation because they are Hamiltonian maps themselves; they can themselves be taken to be the "true" maps. Shadowing theorems address the issue of whether numerical trajectories resemble true trajectories, while lattice maps evade this issue by computing exact trajectories of a map that is closely related to the original one and has the same basic properties. In this sense, lattice maps avoid the need for a shadowing theorem; in addition, lattice maps are cheaper to compute and easier to implement than shadowing calculations. They also apply to systems with any mix of regularity and chaos, while shadowing is only effective in strongly chaotic systems.

8. Conclusions

The structure of iterated mappings that use floating-point arithmetic can be abstracted usefully by the concept of a map-graph. The qualitative predictions concerning the effects of roundoff error, which we made from drawing some map-graphs (fig. 4), are borne out by experiments on a two-dimensional map using `REAL*4` arithmetic; in particular, every trajectory eventually joins a periodic orbit, which we call the limit circuit.

The lattice maps that we have presented provide an alternative to the usual numerical techniques based on floating-point arithmetic that are used to study Hamiltonian maps. The advantage of lattice maps is that they are themselves Hamiltonian maps and they can be iterated an indefinite number of times with no numerical errors.

Lattice maps and shadowing theorems provide the only rigorous methods to establish that long-term numerical computations of chaotic trajectories represent true orbits of a Hamiltonian system. Shadowing theorems justify the use of floating-point calculations over shadowing timescales, while Hamiltonian lattice maps replace a model of a physical system with a similar model that can be evolved exactly over any timescale.

It is interesting that the general features of the phase space structure of orbits are evident from a lattice map with a very coarse grid. As the lattice spacing is decreased, some detailed properties of the original map (such as the transition to global stochasticity in the standard map) are presented with greater precision.

The methods described here are based on the same philosophy as symplectic integration algorithms for Hamiltonian systems [8]. The symplectic integration algorithms ensure that the computed system is Hamiltonian despite truncation error, while the present approach ensures that the computed map is Hamiltonian despite limitations due to roundoff. By combining these methods it is possible to design integration schemes for Hamiltonian flows that ensure the computed system is exactly Hamiltonian despite all numerical errors (and also very accurately represents the system under consideration). We have pointed out a simple first order method in section 5 (see also ref. [25]).

Most modern computers have only four-byte integer arithmetic available in hardware, which limits lattice maps to integers less than about $2^{31} \simeq 2 \times 10^9$. This range can be extended by declaring the integer lattice points to be `REAL*8` variables, in which case integers as large as about $2^{52} \simeq 4.5 \times 10^{15}$ can be used in the lattice[#7].

Our experiments have mostly been based on `REAL*4` floating-point arithmetic and a two-dimensional map. With `REAL*8` arithmetic and more degrees of freedom, the effects of roundoff error will be much smaller and the lengths of the limit circuits will be much longer; however, evolution due to real dynamical effects such as Arnol'd diffusion is also likely to be very slow in many systems of interest. Thus lattice maps can provide welcome reassurance that roundoff errors are not masquerading as dynamical evolution.

Acknowledgements

This research was supported by an operating grant from NSERC, and by NASA Grant NAGW-1448 and NSF Grant AST-8913664. D.E. thanks the Commonwealth Scholarship Commission for financial support. S.T. thanks the California Institute of Technology for their hospitality and the award of a Sherman Fairchild Scholarship. We thank Douglas Heggie, Michel Hénon, and Robert MacKay for comments and discussion.

Appendix

Putting $I_m\begin{pmatrix} X \\ Y \end{pmatrix} = I_m\begin{pmatrix} Z \\ W \end{pmatrix}$ yields $X = Z$ and $Y = W$ so I_m is one-to-one (as in section 5). This simple proof fails for R_b because the floating-point addition operator $\oplus$ does not share all the properties of normal addition.

Lemma. The floating-point map R_b is not one-to-one for any K.

[#7]We are indebted to M. Hénon for this comment.

Proof. Recall the definitions made near expression (2) and eq. (3) in section 1. From (2), if $|A| > 2^{P+1}|B|$ then $A \oplus B = A$. Therefore, if

$$|y| < 2^{-(P+1)}|k_b \otimes \sin_b(p_b \otimes x)| \qquad \text{(A.1)}$$

then $R_b(x, y)$ is independent of y, so if there exists $x \in \mathbb{P}_b$ and two distinct $y \in \mathbb{P}_b$ satisfying (A.1) then R_b is not one-to-one. Similarly, if

$$|y| > 2^{P+1}|k_b \otimes \sin_b(p_b \otimes x)|$$

$$\text{and} \quad |y| > 2^{P+1}x \qquad \text{(A.2)}$$

then $R_b(x, y)$ is independent of x and the existence of two distinct points that have the same y coordinate and satisfy (A.2) will show R_b is many-to-one. If $K \geq 2\pi$ then (A.1) holds, in particular, for $x = 2^{-2}$ and $y \in [0, 2^{-(P+2)}]$. If $K \leq 2\pi$ then (A.2) holds, in particular, for $y = 1$ and $x \in [0, 2^{-(P+2)}]$. (In any practical floating-point arithmetic, the range of e in (2) is always larger than $\{-2, \ldots, 2\}$ so the intervals in question will contain many representable numbers.) Thus R_b is never one-to-one. □

References

[1] E. Allender and M.M. Klawe, Improved lower bounds for the cycle detection problem, Theor. Comput. Sci. 36 (1985) 231–237.

[2] C. Beck, Scaling behaviour of random maps, Phys. Lett. A 136 (1989) 121–125.

[3] C. Beck, and G. Roepstorff, Effects of phase space discretization on the long-time behaviour of dynamical systems, Physica D 25 (1987) 173–180.

[4] G. Benettin, L. Galgani, A. Giorgilli and J.-M. Strelcyn, Lyapunov characteristic exponents for smooth dynamical systems and for Hamiltonian systems; A method for computing all of them. Part 1: Theory, Meccanica (March 1980), 9–20.

[5] G. Benettin, L. Galgani, A. Giorgilli and J.-M. Strelcyn, Lyapunov characteristic exponents for smooth dynamical systems and for Hamiltonian systems; A method for computing all of them. Part 2: Numerical application, Meccanica (March 1980), 21–30.

[6] P.M. Binder and R.V. Jensen, Simulating chaotic behaviour with finite-state machines, Phys. Rev. A 34 (1986) 4460–4463.
[7] N.G. de Bruijn, A combinatorial problem, Kon. Ned. Akad. Wet., Proc. Section of Sciences 49 (1946) 758–764.
[8] P.J. Channell and C. Scovel, Symplectic integration of Hamiltonian systems, Nonlinearity 3 (1990) 231–259.
[9] F.E. Fich, Lower bounds for the cycle detection problem. J. Comput. Syst. Sci. 26 (1983) 392–409.
[10] C. Froeschlé, On the number of isolating integrals in systems with three degrees of freedom, Astrophys. Space Sci. 14 (1971) 110–117.
[11] C. Froeschlé, Numerical study of a four-dimensional mapping, Astron. Astrophys. 16 (1972) 172–189.
[12] C. Froeschlé and J.-P. Scheidecker, On the disappearance of isolating integrals in dynamical systems with more than two degrees of freedom. Astrophys. Space Sci. 25 (1973) 373–386.
[13] R. Gonczi, Fractal dimensions and integrability of Hamiltonian systems: a discretization method, in: The Few Body Problem, ed. M.J. Valtonen (Kluwer, Dordrecht, 1988) pp. 55–59.
[14] C. Grebogi, S.M. Hammel, J.A. Yorke, and T. Sauer, Shadowing of physical trajectories in chaotic dynamics: containment and refinement. Phys. Rev. Lett. 65 (1990) 1527–1530.
[15] B. Harris, Probability distributions related to random mappings, Ann. Math. Stat. 31 (1960) 1045–1062.
[16] C.F.F. Karney, Long time correlations in the stochastic regime, Physica D 8 (1983) 360–380.
[17] D.E. Knuth, 1981. The Art of Computer Programming, Second Ed. Vol. 2: Seminumerical Algorithms, Addison-Wesley, Problems 6 and 12, pp. 7–8; and solutions, pp. 517, 519.
[18] P.D. Lax, Approximation of measure preserving transformations. Commun. Pure Appl. Math. 24 (1971) 133–135.
[19] Y.E. Levy, Some remarks about computer studies of dynamical systems, Phys. Lett. A 88 (1982) 1–3.
[20] A.J. Lichtenberg and M.A. Lieberman, Regular and Stochastic Motion. (Springer, New York, 1983).
[21] J.N. Mather, Non-existence of invariant circles, Ergod. Theor. Dynam. Syst. 4 (1984) 301–309.
[22] J. Moser, Stable and Random Motions in Dynamical Systems (Princeton Univ. Press, Princeton, NJ, 1973).
[23] I. Percival and F. Vivaldi, Arithmetical properties of strongly chaotic motions, Physica D 25 (1987) 105–130.
[24] F. Rannou, Numerical study of discrete plane area-preserving mappings, Astron. Astrophys. 31 (1974) 289–301.
[25] C. Scovel, On symplectic lattice maps. Phys. Lett. A 159 (1991) 396–400.
[26] L.A. Smith, Strange accumulators. Ann. NY Acad. Sci. 497 (1987) 61–65.
[27] J.L. Tennyson, M.A. Lieberman and A.J. Lichtenberg, Diffusion in near-integrable Hamiltonian systems with three degrees of freedom, in: Nonlinear Dynamics and the Beam–Beam Interaction, eds. M. Month and J.C. Herrera, AIP Conf. Proc. No. 57 (American Institute of Physics, New York 1979), p. 272.